ACS APPLIED MATERIALS & INTERFACES

Research Article

www.acsami.org

Synthesis and Isolation of *cis*-2 Regiospecific Ethylene-Tethered Indene Dimer–[70]Fullerene Adduct for Polymer Solar Cell Applications

Ran Tao,[†] Tomokazu Umeyama,[†] Tomohiro Higashino,[†] Tomoyuki Koganezawa,[§] and Hiroshi Imahori*[,†,‡]

[†]Department of Molecular Engineering, Graduate School of Engineering and [‡]Institute for Integrated Cell-Material Sciences (WPI-iCeMS), Kyoto University, Nishikyo-ku, Kyoto 615-8510, Japan

[§]Japan Synchrotron Radiation Research Institute, 1-1-1, Kouto, Sayo-cho, Sayo-gun, Hyogo 679-5198, Japan

Supporting Information

ABSTRACT: Although the utilization of [70]fullerene bis-adducts can enhance the power conversion efficiencies of polymer solar cells (PSCs) owing to their strong absorption intensities and high-lying lowest unoccupied molecular orbital energy levels, this synthetic strategy typically yields a mixture of regioisomers that would mask the intrinsic device performances depending on the substituent pattern on the [70]fullerene derivatives. In this study, a single *cis*-2 regioisomer of C_{70} bis-adduct (*cis*-2-[70]BIEC) has been prepared for the first time by the same strategy that had been applied to [60]fullerene to obtain a regioisomerically pure C_{60} bis-adduct (*cis*-2-[60]BIEC). Diels–Alder reaction was conducted between a rationally designed ethylene-tethered indene dimer and [70]fullerene, followed by isolation using high-performance liquid chromatography suitable for the separation of fullerene derivatives. A series of structural analysis techniques including NMR spectroscopies and X-ray crystallography were used to identify the absolute configuration of the bis-adduct. A systematic study on the optical, electrochemical, and photovoltaic properties of *cis*-2-[70]BIEC as well as the corresponding regioisomer mixture (bis-[70]BIEC) and the monoadduct (*α*-mono-[70]BIEC) has been performed to examine the effect of the pure *cis*-2 regioisomer. More importantly, their properties are compared with those of *cis*-2-[60]BIEC to address the effect of fullerene cage structures, that is, C_{60} versus C_{70}. The PSC based on *cis*-2-[70]BIEC and poly(3-hexylthiophene) showed a remarkable power conversion efficiency of 4.2%, which is higher than those with bis-[70]BIEC (2.2%), *α*-mono-[70]BIEC (2.2%), *cis*-2-[60]BIEC (2.8%), and even a prevalent high-performance C_{70} monoadduct ([70]PCBM, 3.8%). Our synthetic strategy will pave the way for further development on the rational design and isolation of single fullerene bis-adduct regioisomers exhibiting high device performances.

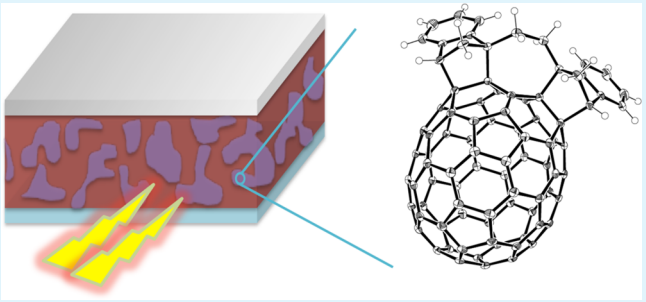

KEYWORDS: *polymer solar cells, fullerenes, C_{70}, bis-adducts, regioisomer, indene, bulk heterojunction*

INTRODUCTION

Fullerene derivatives have been used extensively as electron-acceptors in bulk heterojunction (BHJ) polymer solar cells (PSCs) due to their high electron deficiency and electron mobility.[1−6] The most frequently employed fullerene acceptor is [6,6]-phenyl-C_{61}-butyric acid methyl ester ([60]PCBM), which was first incorporated with poly((2-methoxy-5-(2′-ethylhexyloxy)-*p*-phenylene)vinylene) to form a BHJ structure in 1995.[7] However, power conversion efficiencies (PCEs) of [60]PCBM-based PSCs have been limited by the relatively low lowest unoccupied molecular orbital (LUMO) energy level and weak visible absorption of [60]PCBM. These can be rationalized by the open circuit voltage (V_{OC}) and short circuit current density (J_{SC}) that are highly dependent on the energy difference between the highest unoccupied molecular orbital (HOMO) of the donor and the LUMO of the acceptor and the light-harvesting efficiency, respectively.[1] By increasing the number of the addends on C_{60} from one to two, the LUMO level of bis-[60]PCBM is raised by about 0.1 eV as compared to [60]PCBM. This leads to a 20% increase in V_{OC} (from 0.61 to 0.73 V) of the corresponding PSCs with regioregular poly(3-hexylthiophene) (P3HT) as a donor.[8−10] A decrease of the *π*-conjugation size by the second functionalization on the fullerene sphere makes the electron affinity of fullerene bis-adducts weaker than that of their monoadduct analogues, leading to the increase in the LUMO level and V_{OC}.[8] Meanwhile, a higher J_{SC} value can be expected by replacing C_{60} with C_{70}. By comparison with C_{60}, a lower symmetry of C_{70} (D_{5h} vs I_h) facilitates the lowest-energy transitions, and a drastic increase in its absorption coefficients in visible region is

Received: May 19, 2015
Accepted: July 15, 2015
Published: July 15, 2015

DOI: 10.1021/acsami.5b04351
ACS Appl. Mater. Interfaces 2015, 7, 16676−16685

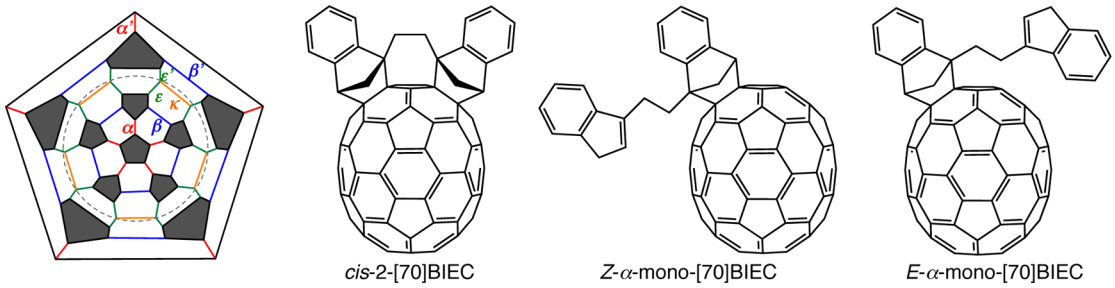

Figure 1. Schlegel diagram of C_{70} showing the distribution of [6,6]-bonds and molecular structures of *cis*-2-[70]BIEC, *Z*-*α*-mono-[70]BIEC, and *E*-*α*-mono-[70]BIEC. *α*-, *β*-, *ε*-, and *κ*-bonds are represented by red, blue, green, and orange lines, respectively. *α*-, *β*-, and *ε*-bonds in the other hemisphere, that is, outside of the dotted circle, are denoted as *α*′, *β*′, and *ε*′.

achievable.[11] Extended *π*-conjugation of C_{70} could lead to a broader absorption profile as well. Up to now, the most successful examples for fullerene bis-adduct acceptors are the Diels−Alder bis-adducts of indene [60]ICBA[12] and its C_{70} analogue [70]ICBA.[13] The optimized PSC devices with P3HT as the donor have achieved the highest PCEs of 7.5%[14] and 7.4%,[15] respectively, among bis-adduct-based PSCs.

Despite their successes, the synthetic strategy by bis-functionalization typically yields a mixture of bis-adduct regioisomers that may impair the device performances related to J_{SC}, V_{OC}, and fill factor (*FF*). It is believed that the random molecular packing and the irregular arrangement of fullerene acceptors in the BHJ structure should disturb charge separation and transport processes.[6,16] It was very recently that the fullerene regioisomer effects on the PSC device performances were investigated in detail.[17−24] Inherently, a C_{60} bis-adduct with two symmetrical same substituents possesses eight regioisomers: *trans*-1, *trans*-2, *trans*-3, *trans*-4, *e*, *cis*-1, *cis*-2, and *cis*-3 isomers. In an earlier work, we designed alkoxycarbonyl-substituted dihydronaphthyl-based [60]-fullerene bis-adducts (NCBA) considering their improved solubility and high polarity that would be beneficial to the facile separation. In fact, we successfully separated *trans*-1, *trans*-2, *trans*-3, *trans*-4, *e*, and a mixture of *cis*-2 and *cis*-3 isomers of NCBA by a preparative high-performance liquid chromatography (HPLC) method with the Buckyprep column.[17,18] A single regioisomer of NCBA generally showed superior device performances to the corresponding regioisomer mixtures. It should be noted, however, that the mixture of *cis*-2 and *cis*-3 isomers was unable to be separated by the HPLC method, and even *cis*-1 was not produced due to the steric hindrance between the two substituents on C_{60}. Nevertheless, *cis*-1, *cis*-2, and *cis*-3 isomers having close proximity of the two substituents on fullerenes would be very attractive because of their plausible more regular close packing with conjugated polymers in the BHJ structure, exhibiting high device performances as a result of "the sterically smallest substituents" to achieve the close contact among the isomers.

Meanwhile, a specific type of fullerene bis-adduct regioisomers can be regioselectively prepared through certain elegant synthetic strategies such as the tether-directed remote functionalization[23−27] and topochemically controlled conversion.[28] In a recent work, we conducted the tether-directed bis-functionalization of C_{60} with an ethylene-bridged indene dimer (1,2-bis(3-indenyl)ethane, BIE) as a reactant to achieve spatially close substituent patterns, that is, *cis*-1, *cis*-2, and *cis*-3 configurations. Indeed, the BIE−C_{60} bis-adduct isomer with the *cis*-2 configuration, *cis*-2-[60]BIEC, was obtained highly regioselectively and isolated for the PSC device application.[19]

Herein, we report on a BIE−C_{70} bis-adduct isomer with the *cis*-2 configuration to study the effects of the pure regioisomer of C_{70} and the fullerene cage structures, that is, C_{60} versus C_{70}. Unlike C_{60} bis-adducts, knowledge about the regiochemistry of C_{70} bis-adducts and their photovoltaic performances is quite limited[28−31] owing to the inherent complexity of the substitution pattern on C_{70} originating from the lower symmetry. As shown in Figure 1, C_{70} has four distinct types of [6,6]-bonds with different local curvature.[32] The reactivity is high in the order of *κ*- < *ε*- < *β*- < *α*-type bonds. According to earlier studies, double functionalizations on C_{70}, no matter in Bingel cyclopropanation or Diels−Alder cycloaddition, prefer to occur at two *α*-bonds in the opposite hemisphere of each other on account of the steric repulsion, forming the *α*−*α*′ pattern C_{70} bis-adducts.[28,30,33,34] The *α*−*β*′ pattern has also been observed albeit in a low possibility.[33,34] Holmes and co-workers isolated a single regioisomer of [70]ICBA with an *α*−*α*′ type configuration, of which PSC device performances were superior to that of the regioisomer mixture of [70]-ICBA.[30] Very recently, Echegoyen et al. synthesized and isolated a bismethano C_{70} derivative attached to *α*-bonds belonging to the same hemisphere with a *cis*-1 configuration through a similar tether-directed remote functionalization method.[31] They also obtained the C_{70} bis-adduct with an *α*−*β* pattern.[31] However, the photovoltaic properties of these tethered bis-adducts of C_{70} were not reported. In this study, we obtained for the first time a C_{70} derivative with two linking indenyl moieties attached to *α*-bonds belonging to the same hemisphere with the *cis*-2 configuration. The replacement of C_{60} with C_{70} is anticipated to increase the absorption in visible region, thereby leading to higher J_{SC} and PCE values. A systematic study on the optical, electrochemical, and photovoltaic properties of the BIE−fullerene C_{70} bis-adduct, that is, *cis*-2-[70]BIEC as well as a regioisomer mixture of BIE−C_{70} bis-adduct (bis-[70]BIEC) and BIE−C_{70} monoadducts with one unreacted indene unit (Figure 1) has been conducted.

EXPERIMENTAL SECTION

Instruments. Fullerene derivative isomers separation was accomplished by Shimadzu Prominence Modular HPLC with Nacalai Tesque Cosmosil buckyprep. ^{1}H NMR and ^{13}C NMR spectra were measured with a JEOL JNM-EX400 NMR spectrometer. High-resolution mass spectra were measured on a JEOL JMS-700 MStation spectrometer. Attenuated total reflectance (ATR) Fourier transform infrared (FT-IR) spectra were recorded on a ThermoFisher Scientific Nicolet 6700 FT-IR. UV−vis absorption spectra were obtained on a PerkinElmer Lambda 900 UV−vis/NIR spectrometer. Single-crystal X-ray diffraction (XRD) analysis data were collected at −150 °C on a Rigaku Saturn70 CCD diffractometer with graphite monochromated Mo−K_α radiation (λ = 0.71069 Å). The structures were solved by

DOI: 10.1021/acsami.5b04351
ACS Appl. Mater. Interfaces 2015, 7, 16676−16685

Scheme 1. Reactions of BIE with C_{70}

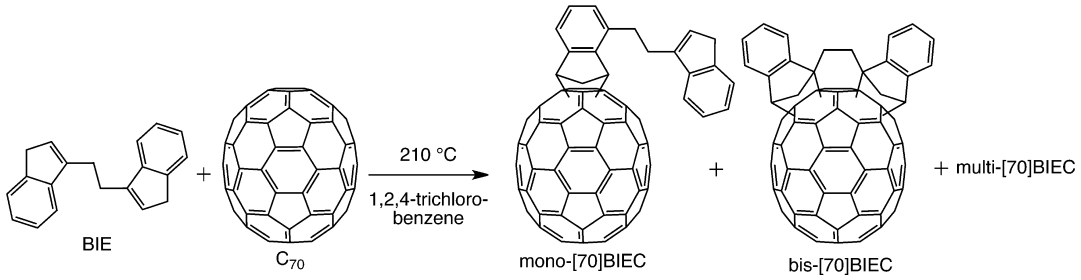

direct method (SHELXS-2014). Cyclic voltammetry (CV) and differential pulse voltammetry (DPV) measurements were performed using an ALS 630A electrochemical analyzer in an *o*-dichlorobenzene/acetonitrile mixture (v/v = 5:1) containing 0.1 M tetrabutylammonium hexafluorophosphate (Bu_4NPF_6) as a supporting electrolyte. Thermogravimetric analysis (TGA) measurements were conducted with a SHIMADZU TGA-50 under flowing nitrogen at a scan rate of 10 °C min^{-1}. Differential scanning calorimetry (DSC) analyses were made on a SHIMADZU DSC-60 under flowing nitrogen at a scan rate of 10 °C min^{-1}. Atomic force microscopy (AFM) analyses were carried out with an Asylum Technology MFP-3D-SA in the AC mode. Photoluminescence (PL) spectra measurements were recorded with a HORIBA SPEX Fluoromax-3. XRD analyses of film samples were carried out with a Rigaku SmartLab 9 kW using Cu K_α radiation. Samples for the X-ray measurements were prepared by spin-coating the P3HT:fullerene solution on the ITO/PEDOT:PSS substrate. Solvent and thermal annealing was conducted after the spin-coating. Photocurrent−voltage characteristics were measured by Keithley 2400 SourceMeter under an argon atmosphere and simulated solar light (100 mW cm^{-2}, AM1.5) with OTENTO-SUN III solar simulator (Bunkoukeiki). Photocurrent action spectra were recorded with CEP-2000RR (Bunkoukeiki). Current−voltage characteristics of the electron-only devices for space-charge-limited current (SCLC) measurements were conducted using Keithley 2400 SourceMeter under an argon atmosphere.

Materials. P3HT, C_{70} (98.0%), [70]PCBM (99.0%), and [70]ICBA (99%) were obtained from Sigma-Aldrich, MTR Ltd., American Dye Source, Inc., and Solenne BV and used as received. Other chemicals and solvents were of reagent-grade quality, purchased commercially, and used without further purification unless otherwise noted. Thin-layer chromatography (TLC) and column chromatography were performed with silica gel 60 F_{254} (Merck) and SiliaFlash F60 (230−400 mesh; SiliCycle Inc.), respectively. The procedure for the synthesis of BIE was described in the previous report.[19,35]

Synthesis. BIE−C_{70} adducts ([70]BIEC): BIE (0.88 g, 3.4 mmol) and C_{70} (3.14 g, 3.7 mmol) were dissolved in 1,2,4-trichlorobenzene (150 mL) and stirred at 210 °C for 48 h under an argon atmosphere. Subsequently, the reaction mixture was poured into CH_3OH (800 mL) and filtrated. The residue was dissolved with CS_2 and adsorbed on silica gel. Four fractions with main components of unreacted C_{70} (>2.40 g), BIE−C_{70} adducts with one unreacted indene unit (mono-[70]BIEC, 0.48 g), a regioisomer mixture of BIE−C_{70} adducts with no unreacted indene units (bis-[70]BIEC, 0.35 g), and multiple-BIE−C_{70} adducts (multi-[70]BIEC) were eluted sequentially in this order with hexane/toluene = 2:1 (v/v) as an eluent. The third and second fractions were further subjected to preparative HPLC with Buckyprep column (Figure S1 in the Supporting Information) to afford the regioisomerically pure *cis*-2-[70]BIEC (0.31 g, 32% yield based on the amount of reacted C_{70}) and an α type mono-[70]BIEC (α-mono-[70]BIEC, 0.45 g, 46% yield).

BIE−C_{70} adducts were also prepared through a solvent-free procedure as follows. The vessel loaded with BIE (0.26 g, 1.0 mmol) and C_{70} (0.93 g, 1.1 mmol) was vacuumed and then heated at 240 °C for 2.5 h. The reaction mixture was cooled down and dissolved with CS_2. The unreacted C_{70}, mono-[70]BIEC (0.25 g), *cis*-2-[70]BIEC (0.01 g), and multi-[70]BIEC with unreacted indene units (0.12 g) were eluted sequentially in this order by silica gel column chromatography with hexane/toluene = 2:1.

cis-2-[70]BIEC. ^{1}H NMR ($C_2D_2Cl_4$, 400 MHz): δ7.75 (d, 1H), 7.47 (t, 2H), 7.40 (t, 2H), 7.33 (m, 3H), 4.42 (s, 1H), 4.21 (s, 1H), 3.64 (t, 1H), 2.97 (q, 1H), 2.77 (q, 1H), 2.59 (m, 2H), 2.22 (m, 2H), 2.16 (d, 1H). ^{13}C NMR ($C_2D_2Cl_4$, 400 MHz): δ 160.59, 159.18, 156.81, 152.21, 152.08, 151.77, 151.69, 151.04, 149.84, 149.37, 149.24, 149.10, 148.70, 148.60, 148.38, 148.17, 147.86, 147.38, 147.12, 146.64, 146.57, 146.18, 145.98, 145.58, 145.24, 144.76, 143.50, 142.58, 142.47, 142.34, 141.74, 141.57, 138.51, 135.90, 135.60, 135.16, 134.87, 134.55, 134.12, 133.96, 133.75, 132.36, 130.68, 127.70, 127.42, 127.05, 126.92, 125.38, 123.22, 122.81, 121.21, 118.99, 69.29, 68.92, 66.21, 66.07, 65.09, 64.25, 55.41, 53.47, 52.77, 48.75, 28.66, 25.62. IR (ATR): ν_{max}/cm^{-1} 3045, 3017, 2940, 2911, 2898, 2869, 2838, 1556, 1505, 1453, 1420, 1407, 1327, 1269, 1221, 1123, 1042, 1014, 972, 931, 852, 791, 752, 729, 717, 694. HRMS (APCI): calcd for $C_{90}H_{18}$[M + H] 1099.1481, found 1099.1477. Crystallographic data: $C_{90}H_{18}$·CS_2, M_r = 1175.17, monoclinic, space group $P2_1/n$ (no. 14), a = 14.6016(18), b = 17.352(2), c = 19.712(3) Å, β = 106.4970(13)°, V = 4788.6(10) $Å^3$, T = 123(2) K, Z = 4, ρ_{calc} = 1.630 g cm^{-3}, R_1 = 0.0687 [$I > 2\sigma(I)$], R_w (all data) = 0.632, GOF = 1.062. CCDC-1064104 contains the supplementary crystallographic data for this paper. These data can be obtained free of charge from The Cambridge Crystallographic Data Centre via www.ccdc.cam.ac.uk/data_request/cif.

α-mono-[70]BIEC. ^{1}H NMR ($C_2D_2Cl_4$, 400 MHz): δ7.62 (d), 7.50 (m), 7.49 (d), 7.40−7.24 (m), 6.59 (s), 6.26 (s), 4.74 (s), 4.29 (s), 3.54 (t), 3.45 (s), 3.27 (s), 3.19 (m), 3.07 (t), 2.90 (m), 2.61 (m), 2.54 (d). ^{13}C NMR ($CDCl_3$/ CS_2, 400 MHz): δ 159.03, 158.66, 157.80, 157.62, 156.00, 155.38, 155.11, 151.20, 151.10, 151.07, 151.02, 150.76, 150.74, 150.65, 150.53, 150.44, 150.40, 150.35, 150.31, 150.26, 149.97, 149.93, 149.69, 149.48, 149.41, 149.40, 149.36, 148.99, 148.94, 148.89, 148.72, 148.67, 148.44, 148.41, 148.38, 148.36, 147.53, 147.20, 147.14, 147.06, 147.02, 146.71, 146.67, 146.57, 146.36, 145.98, 145.91, 145.88, 145.83, 145.59, 145.53, 145.23, 145.14, 144.82, 144.66, 144.57, 144.11, 144.01, 143.84, 143.06, 143.01, 142.90, 142.83, 142.75, 142.59, 142.44, 142.41, 141.78, 141.45, 139.47, 139.44, 138.45, 137.93, 133.76, 133.31, 133.22, 133.20, 131.01, 130.87, 130.83, 130.80, 127.85, 127.68, 127.13, 127.08, 126.99, 126.12, 125.99, 124.84, 124.74, 124.04, 123.77, 123.65, 123.630 122.67, 122.44, 118.71, 118.53, 64.90, 63.71, 56.85, 54.59, 47.96, 47.61, 38.00, 37.80, 29.89, 29.20, 24.74. IR (ATR): ν_{max}/cm^{-1} 3066, 2945, 2906, 2865, 1554, 1505, 1451, 1422, 1389, 1319, 1280, 1247, 1217, 1152, 1124, 1016, 960, 937, 910, 864, 793, 757, 733, 711. HRMS (APCI): calcd for $C_{90}H_{18}$[M + H] 1099.1481, found 1099.1419.

Quantum Chemical Calculation. Geometry optimization and electronic structure calculations for the fullerene compounds were performed using density functional theory (DFT) at the RB3LYP/6-31G (d) level. Chemical shift values were further simulated with the Gauge-Independent Atomic Orbital (GIAO) method at the B3LYP/6-31G (d) level after the geometry optimization. The ^{1}H chemical shift values were calculated relative to tetramethylsilane (TMS) (δ = 0.00 ppm, absolute shielding: 32.18 ppm). The calculations were carried out with Gaussian 09 software package using a spin-restricted formalism.[36]

Device Fabrication. PSC devices were fabricated as follows. An indium tin oxide (ITO) glass substrate with a sheet resistance of 5 Ω/

DOI: 10.1021/acsami.5b04351
ACS Appl. Mater. Interfaces 2015, 7, 16676−16685

sq (Geomatec) was used. The substrates were ultrasonically cleaned with detergent, deionized water, 2-propanol, and ethanol consecutively. After dried and UV−ozone treated, the substrates were spin-coated with poly(ethylene dioxythiophene) doped with polystyrene sulfonic acid (PEDOT:PSS, Clevios P VP AI 4083) at 1000 rpm for 60 s and dried at 200 °C for 10 min. Then, a mixed solution of P3HT (12 mg mL^{-1}) and the fullerene derivative (7.2 mg mL^{-1}) in *o*-dichlorobenzene was spin-coated onto the PEDOT:PSS layer under an argon atmosphere. The blend films were put in a glass Petri dish to undergo solvent annealing and then on a 150 °C hot plate for 8 min to go through thermal annealing. The thicknesses of these blend films were about 90 nm. Finally, Ca (20 nm) and Al (100 nm) layers were successively deposited under high vacuum (ca. 10^{-4} Pa). During the photovoltaic measurements, a nonreflective black aperture was attached to define the active area and avoid the scattering effect of incident light.

Electron-only devices were fabricated as follows. An Al film (50 nm) was first thermally deposited onto the glass substrate. The P3HT:fullerene blend film with a thickness of 110−130 nm was spin-coated on the deposited Al film. Finally, the active layer was capped by an Al electrode (100 nm).

RESULTS AND DISCUSSION

Synthesis and Isolation. The synthesis and isolation of the BIE−C_{70} adducts have been conducted, as described for the BIE−C_{60} adducts (Scheme 1).[19] Diels−Alder reaction between BIE and C_{70} in refluxing 1,2,4-trichlorobenezene resulted in four fractions, that is, unreacted C_{70}, BIE−C_{70} monoadducts with one unreacted indene unit (mono-[70]BIEC), a regioisomer mixture of BIE−C_{70} adducts with no unreacted indene units (bis-[70]BIEC), and multiple-BIE−C_{70} adducts (multi-[70]BIEC), which were eluted sequentially in this order by the silica gel chromatography with hexane/toluene = 2:1 (v/v) as an eluent. Further purification of the third fraction by HPLC equipped with Buckyprep column (Figure S1a in the Supporting Information) afforded a regioisomerically pure *cis*-2 isomer, *cis*-2-[70]BIEC as a major product in an overall yield of 32% based on the amount of reacted C_{70}. In addition, the second fraction was also subjected to the HPLC purification (Figure S1b in the Supporting Information). An *α*-type mono-[70]BIEC (*α*-mono-[70]BIEC) consisting of two stereoisomers was obtained in 46% yield. The overall yields of the *cis*-2 bis-adduct and the monoadduct of the BIE−C_{70} are low and high, respectively, compared to those of the BIE−C_{60} adducts (48% and 2%, respectively). According to frontier molecular orbital theory, a cyclopentadiene unit of thermally generated isoindene from an indene unit prefers to attack the carbon atoms of fullerenes with larger LUMO coefficients.[37] Thus, the second Diels−Alder reaction of each BIE unit may be hindered by the lower LUMO electron density at the neighboring *α*-type [6,6]-bonds of mono-[70]BIEC in comparison with mono-[60]BIEC (for details in the LUMO electron density distribution, see the theoretical calculation part in the ensuing paragraphs).

It should be noted here that solvent-free Diels−Alder reaction of C_{60} with BIE in the melted state under vacuum at 240 °C yielded *cis*-2-[60]BIEC and multi-[60]BIEC without forming mono-[60]BIEC and the other regioisomers of the BIE−C_{60} bis-adducts.[19] Although the total yield of *cis*-2-[60]BIEC is relatively low (10%), this method has the advantage that the regioisomerically pure *cis*-2-[60]BIEC can be obtained without the HPLC separation. In contrast, solvent-free Diels−Alder reaction of C_{70} with BIE in the melted state under vacuum at 240 °C only yielded a trace amount of *cis*-2-[70]BIEC, providing mono-[70]BIEC and multi-[70]BIEC with unreacted indene units as main products. The second Diels−Alder reaction of each BIE unit at the [70]fullerene cage was hindered, as is the case with the reaction in solution.

Structural Characterizations and Optical Properties. Molecular structures of *α*-mono-[70]BIEC and *cis*-2-[70]BIEC were characterized by UV−vis absorption spectra, ^1H and ^{13}C NMR spectra, FT-IR spectroscopy, and high-resolution mass spectrometry. The ascription of the BIE−C_{70} monoadduct to *α*-mono-[70]BIEC, where one *α*-type [6,6]-bond of C_{70} is reacted with BIE, is supported by the typical absorption profile of *α*-type C_{70} monoadducts with characteristic peaks at around 400 and 460 nm (Figure 2).[29,32] The ^1H NMR spectrum of *α*-

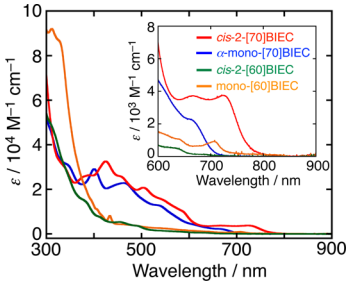

Figure 2. UV−vis absorption spectra of *cis*-2-[70]BIEC (red), *α*-mono-[70]BIEC (blue), *cis*-2-[60]BIEC (green), and mono-[60]BIEC (orange) in *o*-dichlorobenzene. The insets depict the enlarged absorption spectra from 600−900 nm.

mono-[70]BIEC exhibits two sets of vinyl resonances at 6.26 and 6.59 ppm arising from the intact indene unit and methine protons of the bridgehead at 4.74 and 4.29 ppm both in a peak area ratio of 0.9:1 (Figure S2 in the Supporting Information). This result indicates the presence of the achiral stereoisomers, in which the intact indene units are pointing to the opposite directions (denoted as *Z*-*α*-mono-[70]BIEC and *E*-*α*-mono-[70]BIEC, as illustrated in Figure 1). These *Z* and *E* isomers have close properties that make them inseparable by the HPLC technique. In contrast, vinyl resonances are absent in the ^1H NMR spectrum of *cis*-2-[70]BIEC, while two methine peaks with a peak area ratio of 1:1 appear at 4.42 and 4.21 ppm (Figure S3 in the Supporting Information), verifying the occurrence of the bis-functionalization. The assignments of the NMR peaks were further supported by DFT calculation with the GIAO method at the optimized structure (Figure S4 in the Supporting Information). The simulated chemical shifts are largely consistent with the experimental values. The amount of *E*-*α*-mono-[70]BIEC is found to be slightly larger than that of *Z*-*α*-mono-[70]BIEC in *α*-mono-[70]BIEC (*Z*:*E* = 0.9:1).

The structure of *cis*-2-[70]BIEC was unequivocally identified by X-ray crystallography (Figure 3a). Two *α*-type [6,6]-bonds emanating from the same polar pentagon are saturated by the double Diels−Alder reactions between C_{70} and the BIE addend. Since these two *α*-type bonds do not belong to the same hexagon, the structure is denoted as the *cis*-2 isomer of C_{70} bis-adducts. Two methylene bridges of the indene addends are protruding on the same side as seen in *cis*-2-[60]BIEC,[19] resulting in a *meso* compound. The packing diagram reveals the short contacts between the C_{70} moieties in the *cis*-2-[70]BIEC crystal (Figure 3b; Figure S5a in the Supporting Information). Compared to the *cis*-2-[60]BIEC molecules, however, the shortest distance between the C_{70} ellipsoids is slightly long (3.28 Å vs 3.08 Å). The formation of the arranged rows of contacted fullerene pairs, which is observed in the crystal of *cis*-

DOI: 10.1021/acsami.5b04351
ACS Appl. Mater. Interfaces 2015, 7, 16676−16685

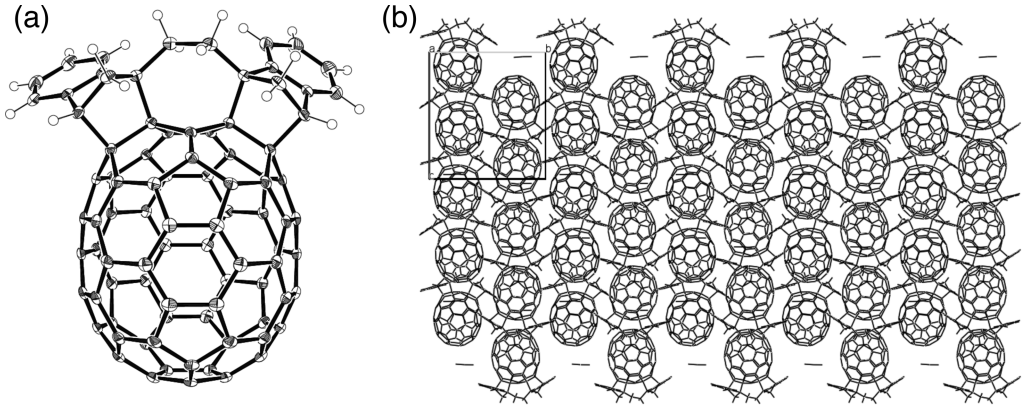

Figure 3. (a) X-ray crystal structure, where thermal ellipsoids represent 50% probability, and solvent molecules are omitted for clarity; and (b) packing structures with solvent molecules along the *a*-axis for *cis*-2-[70]BIEC obtained from CS_2.

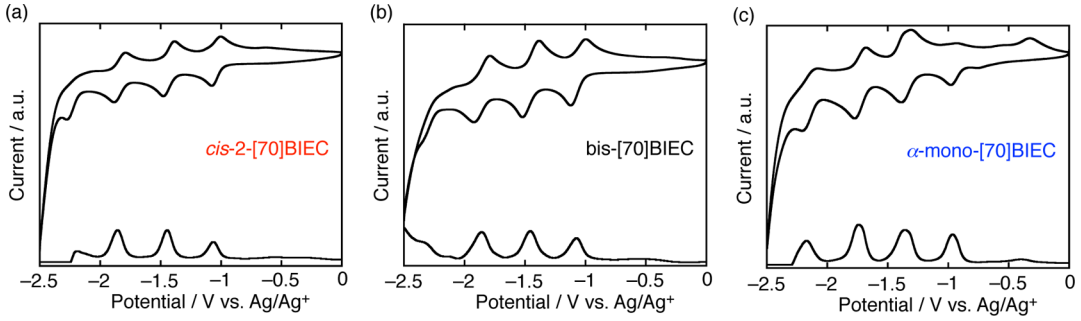

Figure 4. Cyclic voltammograms (upper) and differential pulse voltammograms (lower) of (a) *cis*-2-[70]BIEC, (b) bis-[70]BIEC, and (c) *α*-mono-[70]BIEC versus a reference electrode of Ag/Ag^+ (0.01 M $AgNO_3$) measured in *o*-dichlorobenzene/acetonitrile mixture (v/v = 5:1) containing 0.1 M tetrabutylammonium hexafluorophosphate (Bu_4NPF_6). Sweep rate: 0.1 V s^{-1}; reference electrode, Ag/Ag^+ (0.01 M $AgNO_3$, 0.09 M Bu_4PF_6 in acetonitrile).

2-[60]BIEC,[19] is missing from the *cis*-2-[70]BIEC crystal. Besides, only $\pi-\pi$ interactions between the $C_{70}-C_{70}$ spheres are found in the crystal packing of *cis*-2-[70]BIEC, whereas additional $\pi-\pi$ interactions between the C_{60} sphere and the phenyl group of the neighboring addend exist among the *cis*-2-[60]BIEC molecules. This suggests the possibility of the formation of another electron-transporting channel in the active layer consisting of P3HT and *cis*-2-[60]BIEC (Figure S5b in the Supporting Information). These results indicate that *cis*-2-[70]BIEC has a lower electron mobility than *cis*-2-[60]BIEC in the composite films with P3HT (vide infra).

Molar absorption coefficients of *cis*-2-[70]BIEC and *α*-mono-[70]BIEC between 400 and 700 nm are markedly increased in comparison with *cis*-2-[60]BIEC and mono-[60]BIEC (Figure 2). Especially, the absorption edge of *cis*-2-[70]BIEC is located at 780 nm, which is red-shifted relative to *α*-mono-[70]BIEC and other C_{70} bis-adduct isomers.[28,30,31,38] This can be ascribed to the structural distortion of the C_{70} ellipsoid caused by the steric addend. This superior optical property should make *cis*-2-[70]BIEC an excellent light-absorbing agent in the BHJ structure and in turn result in higher J_{SC} in the *cis*-2-[70]BIEC-based device than the other fullerenes-based ones.

Electrochemical Properties, Theoretical Calculations, and Thermal Properties. Electrochemical properties of the BIE−C_{70} adducts were evaluated by CV and DPV measurements (Figure 4). The first (E_1), second (E_2), and third (E_3) reduction potentials determined from the DPV peaks[18] are listed in Table 1 together with those of the prevalent C_{70} monoadduct acceptor, [70]PCBM. The LUMO energy levels[39]

Table 1. Reduction Potentials and LUMO Energy Levels

fullerene	E_1 (V)[a]	E_2 (V)[a]	E_3 (V)[a]	LUMO[b](eV)
cis-2-[70]BIEC	−1.06	−1.44	−1.86	−3.54
bis-[70]BIEC	−1.07	−1.46	−1.86	−3.53
α-mono-[70]BIEC	−0.96	−1.36	−1.74	−3.64
[70]PCBM	−0.91	−1.30	−1.69	−3.69

[a]Values are versus Ag/Ag^+ (0.01 M $AgNO_3$). [b]LUMO = −e[4.80 + (E_1 − E_{Fc})] eV; E_{Fc} is the potential for ferrocene/ferrocenium (Fc/Fc^+) couple.[39]

of *cis*-2-[70]BIEC and bis-[70]BIEC are 0.10−0.16 eV higher than those of *α*-mono-[70]BIEC and [70]PCBM, as in the case of *cis*-2-[60]BIEC and bis-[60]BIEC,[19] which would be desirable for the photovoltaic application in PSCs to improve V_{OC}.[1]

To get more insight into the electronic structures of the fullerene derivatives, we performed DFT calculations using RB3LYP/6-31G (d) model. The LUMO levels were obtained after the geometry optimizations, as illustrated in Figure 5. The differences in the theoretical LUMO levels between the fullerene derivatives largely agree with those obtained from the electrochemical measurements (Table 1).[19] The HOMO level of *cis*-2-[70]BIEC is higher than those of the other fullerenes, yielding a relatively small theoretical bandgap of 2.33 eV compared to *Z*-*α*-mono-[70]BIEC (2.53 eV), *E*-*α*-mono-[70]BIEC (2.52 eV), *cis*-2-[60]BIEC (2.60 eV), and mono-[60]BIEC (2.55 eV). This result corroborates the aforementioned experimental redshift of *cis*-2-[70]BIEC in the UV−vis absorption spectrum (Figure 2). The electron densities of all

DOI: 10.1021/acsami.5b04351
ACS Appl. Mater. Interfaces 2015, 7, 16676−16685

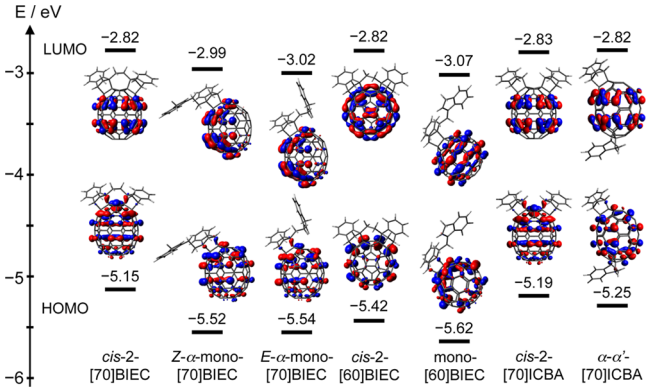

Figure 5. Optimized geometries, HOMO/LUMO electron density distributions, and energy levels of *cis*-2-[70]BIEC, *Z*-α-mono-[70]BIEC, *E*-α-mono-[70]BIEC, *cis*-2-[60]BIEC, mono-[60]BIEC, *cis*-2-[70]ICBA, and α−α′-[70]ICBA simulated by DFT calculations using RB3LYP/6-31G(d) model.

the HOMOs and LUMOs of the fullerene bis-adduct isomers are primarily localized in the fullerene cores, but the distribution pattern of the electron densities varies (Figure 5). With respect to the LUMO configuration, *cis*-2-[60]BIEC and mono-[60]BIEC show rather delocalized electron densities throughout the whole of the fullerene moiety, whereas *cis*-2-[70]BIEC and α-mono-[70]BIEC prefer relatively localized electron distributions at the fullerene cage. Additionally, the LUMO of α-mono-[70]BIEC scarcely resides at the α-type [6,6]-bonds with *cis*-2 configuration, which leads to a lower reactivity of the second Diels−Alder addition than mono-[60]BIEC (Figure S6 in the Supporting Information). This is in good agreement with the experimental results that the overall yields of the *cis*-2 bis-adduct and the monoadduct of C_{70}−BIE adducts are low and high, respectively, compared to those of the C_{60}−BIE adducts. With regard to the HOMO configuration, the contribution of the BIE addend to the electron density of *cis*-2-[70]BIEC is not negligible, thereby dramatically upshifting the HOMO level and narrowing the bandgap. In particular, the theoretical HOMO energy level of *cis*-2-[70]BIEC is higher than the other indene bis-adducts of C_{70}, that is, 0.04 eV higher than *cis*-2-[70]ICBA without the ethylene tether and 0.10 eV higher than α−α′-[70]ICBA with the 2 o'clock configuration,[30] although the theoretical LUMO levels of these molecules are almost identical (Figure 5). Therefore, the superiority of *cis*-2-[70]BIEC in the UV−vis absorption can be ascribed to its unique α−α regiochemical pattern and the structural distortion originated from the ethylene tether.

The thermal stability of *cis*-2-[70]BIEC was evaluated by TGA (Figure S7 in the Supporting Information). *cis*-2-[70]BIEC displays high thermal stability with an onset point of steep weight losses at about 340 °C, which is comparable with that of *cis*-2-[60]BIEC (350 °C) and higher than that of mono-[60]BIEC (310 °C).[19] The steep weight losses correspond to the detachment of BIE groups, that is, retro-Diels−Alder reaction, and the dual attachment in *cis*-2-[70]BIEC and *cis*-2-[60]BIEC leads to the higher thermal stabilities. With respect to DSC behaviors, *cis*-2-[70]BIEC retains featureless heat flows, which is in sharp contrast to *cis*-2-[60]BIEC and mono-[60]BIEC with crystallization peaks at 154 and 167 °C.[19] As a result, *cis*-2-[70]BIEC presumably is able to stay amorphous after the thermal annealing treatment during the PSC device fabrication, while *cis*-2-[60]BIEC and mono-[60]BIEC may undergo crystallization, yielding large phase separation between the donor and the acceptor.[40−42]

Photovoltaic Properties. PSCs based on the ITO/PEDOT:PSS/P3HT:fullerene/Ca/Al configuration were fabricated to evaluate the photovoltaic performances of the different fullerene adducts. The detailed device-fabrication process is described in the Experimental Section. The current density−voltage characteristics are shown in Figure 6, panel a,

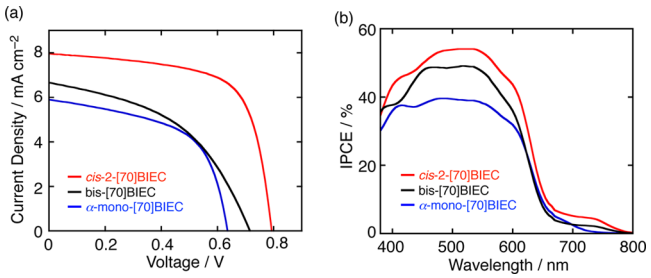

Figure 6. (a) Current density−voltage curves and (b) photocurrent action spectra of PSC devices based on P3HT:*cis*-2-[70]BIEC (red), P3HT:bis-[70]BIEC (black), and P3HT:α-mono-[70]BIEC (blue). The convolution of the spectral response in panel b with the photon flux of the AM 1.5G spectrum provided the estimated J_{SC} values of 7.92, 6.81, and 5.84 mA cm^{-2}, respectively.

and the averaged photovoltaic parameters are listed in Table 2. Since the solubility of *cis*-2-[70]BIEC in *o*-dichlorobenzene is lower than that of *cis*-2-[60]BIEC, the optimized weight ratio of the fullerene derivative in the mixed solution with P3HT is lower in P3HT:*cis*-2-[70]BIEC ([P3HT]:[*cis*-2-[70]BIEC] = 1:0.6) than in P3HT:*cis*-2-[60]BIEC ([P3HT]:[*cis*-2-[60]BIEC] = 1:0.8).[19] Note that the P3HT:*cis*-2-[70]BIEC system was optimized by altering the annealing conditions (temperature: 100−180 °C, time: 5−15 min). The best photovoltaic performance was obtained when the device was annealed at 150 °C for 8 min. We used the weight ratios of [P3HT]:[fullerene] = 1:0.6 and the annealing condition of 150 °C for 8 min for all the C_{70}-based fullerene derivatives in this study.

Comparison of C_{70}-Based Fullerene Derivatives. As is the case with BIE−C_{60} adducts,[19] the superior photovoltaic performance of the *cis*-2 bis-adduct was exemplified in the C_{70}-based fullerene derivatives (Figure 6a and Table 2). The PSC device with *cis*-2-[70]BIEC exhibits a remarkable PCE value of 4.2%, which is higher than the devices with P3HT:bis-[70]BIEC (2.2%), α-mono-[70]BIEC (2.2%), and even a prevalent high-performance C_{70} monoadduct, [70]PCBM (3.8%), under the same condition for the device fabrication. As expected, the V_{OC} values of the PSCs with *cis*-2-[70]BIEC (0.79 V) and bis-[70]BIEC (0.72 V) are higher than those with α-mono-[70]BIEC (0.64 V) and [70]PCBM (0.60 V) owing to the elevated LUMO levels by the bis-functionalization. It is noteworthy that a slight increase in the V_{OC} value of the P3HT:α-mono-[70]BIEC-based device relative to the P3HT:[70]PCBM-based one reflects the difference in the LUMO energy levels (Table 1). A similar phenomenon has been observed with other Diels−Alder fullerene adducts, in which the cofacial π-orbital interactions between the fullerene orbitals and the aromatic addend ring decrease the electron affinity and thereby increase the LUMO energy level.[12,13,43] The J_{SC} values of the P3HT:bis-[70]BIEC- and P3HT:α-mono-[70]BIEC-

DOI: 10.1021/acsami.5b04351
ACS Appl. Mater. Interfaces 2015, 7, 16676−16685

Table 2. Device Characteristics of PSCs[a]

acceptor	J_{SC} (mA cm^{-2})	V_{OC} (V)	*FF*	PCE (%)	mobility[b] (cm^2 V^{-1} s^{-1})
cis-2-[70]BIEC	7.95 ± 0.18	0.79 ± 0.01	0.67 ± 0.01	4.2 ± 0.2	3.0×10^{-7}
bis-[70]BIEC	6.66 ± 0.34	0.72 ± 0.02	0.46 ± 0.02	2.2 ± 0.2	1.2×10^{-7}
α-mono-[70]BIEC	5.90 ± 0.34	0.64 ± 0.01	0.57 ± 0.02	2.2 ± 0.2	1.6×10^{-6}
[70]PCBM	8.60 ± 0.16	0.60 ± 0.01	0.73 ± 0.01	3.8 ± 0.1	2.0×10^{-5}
[70]ICBA	9.30 ± 0.43	0.85 ± 0.01	0.61 ± 0.03	4.8 ± 0.2	3.3×10^{-5}

[a]The photovoltaic parameters are average values from more than six independent solar cells. The repeatability of the PCE values for the PSCs was confirmed. [b]Estimated by the SCLC method.

based devices (6.66 and 5.90 mA cm^{-2}) were lower than that of the P3HT:*cis*-2-[70]BIEC-based one (7.95 mA cm^{-2}), irrespective of the comparable light-harvesting efficiency (Figure 7). The SCLC electron mobility of the P3HT:*cis*-2-[70]BIEC composite film (3.0×10^{-7} cm^2 V^{-1} s^{-1}) is higher than that of the P3HT:bis-[70]BIEC film (1.2×10^{-7} cm^2 V^{-1} s^{-1}) but lower than that of P3HT:α-mono-[70]BIEC (1.6×10^{-6} cm^2 V^{-1} s^{-1}). This counterintuitive result suggests that the charge collection efficiency is not a determinant of the difference in J_{SC} values of the BIEC–C_{70} adducts, and the other factors such as charge separation efficiency are crucial. On the other hand, the device with a regioisomer mixture of C_{70}-indene bis-adducts, that is, [70]ICBA, showed a rather higher device performance (4.8%) than *cis*-2-[70]BIEC under the same condition for the device fabrication (Table 2).[15,30] This difference may result from the much higher electron mobility of P3HT:[70]ICBA (3.3×10^{-5} cm^2 V^{-1} s^{-1}) than that of the P3HT:*cis*-2-[70]BIEC composite film by a factor of more than one-hundred.

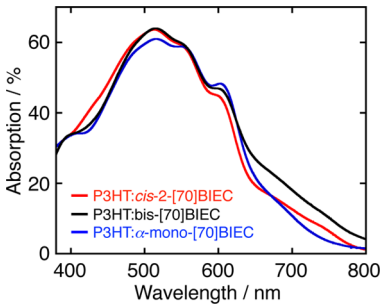

Figure 7. UV–vis absorption spectra of the P3HT:*cis*-2-[70]BIEC (red), P3HT:bis-[70]BIEC (black), and P3HT:α-mono-[70]BIEC (blue) composite films. The absorption arising from ITO and PEDOT:PSS was subtracted.

Comparison of C_{60} and C_{70}-Based Derivatives. The current density–voltage curves, photocurrent action spectra, and UV–vis absorption spectra of the P3HT:*cis*-2-[70]BIEC and P3HT:*cis*-2-[60]BIEC composite films are shown for comparison in Figure S8 in the Supporting Information. Although the V_{OC} values for *cis*-2-[70]BIEC and *cis*-2-[60]BIEC are almost identical, a significant enhancement of the J_{SC} values from 6.60–7.95 mA cm^{-2} is witnessed after the replacement of C_{60} with C_{70} (Table 2; Figure S8a in the Supporting Information).[19] Consistently, the *cis*-2-[70]BIEC-based device shows higher IPCE values than the *cis*-2-[60]BIEC-based one in the wavelength region of >530 nm (Figure S8b in the Supporting Information). This enhancement in the J_{SC} value of the *cis*-2-[70]BIEC-based device can mainly stem from the improvement in the absorption of the photoactive layer (Figure S8c in the Supporting Information). Considering the comparable film thicknesses of the photoactive layers (ca. 90 nm), the improvement in the light-harvesting efficiency is attributable to the higher molar extinction coefficient of *cis*-2-[70]BIEC than *cis*-2-[60]BIEC. A noticeable increase of the IPCE values at 670–800 nm results from the significant absorption by *cis*-2-[70]BIEC at the long wavelength region. It should also be stated here that the electron mobilities of *cis*-2-[70]BIEC, bis-[70]BIEC, and α-mono-[70]BIEC (Table 2) are lower than those of *cis*-2-[60]BIEC, bis-[60]BIEC, and mono-[60]BIEC (3.5×10^{-5}, 2.5×10^{-5}, and 2.7×10^{-5} cm^2 V^{-1} s^{-1}, respectively).[19] The lower symmetrical fullerene cage structure of C_{70} than C_{60} would hinder the formation of closely packed structures of the C_{70} derivatives, as suggested from the packing structure of *cis*-2-[70]BIEC (Figure 3; Figure S5 in the Supporting Information).[19] The lower weight ratio of the C_{70} derivatives than the C_{60} ones in the composite films would also inhibit the construction of electron transportation pathways, causing a decrease in the charge collection efficiency of the C_{70} derivative-based devices. Nevertheless, owing to the enhancements in the light-harvesting efficiency and J_{SC}, *cis*-2-[70]BIEC can achieve a notably higher PCE value (4.2%) than *cis*-2-[60]BIEC (2.8%). Similarly, higher J_{SC} and PCE values are obtained with bis-[70]BIEC (6.66 mA cm^{-2} and 2.2%) and α-mono-[70]BIEC (5.90 mA cm^{-2} and 2.2%) when compared to bis-[60]BIEC (4.70 mA cm^{-2} and 1.8%) and mono-[60]BIEC

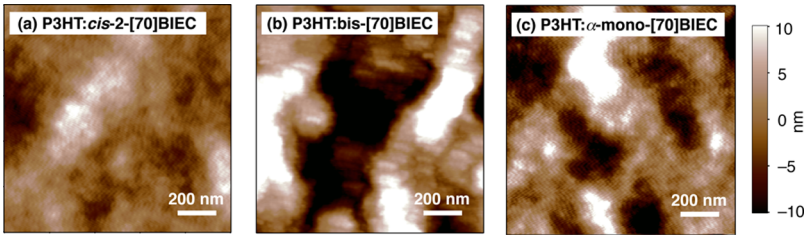

Figure 8. Tapping-mode atomic force micrographs of (a) P3HT:*cis*-2-[70]BIEC, (b) P3HT:bis-[70]BIEC, and (c) P3HT:α-mono-[70]BIEC. The color scale represents the height topography, with bright and dark representing the highest and lowest features, respectively. The rms surface roughnesses are (a) 3.4, (b) 8.1, and (c) 6.4 nm, respectively.

DOI: 10.1021/acsami.5b04351
ACS Appl. Mater. Interfaces 2015, 7, 16676–16685

(5.15 mA cm^{-2} and 1.6%).[19] These results reveal the obvious advantage of the utilization of C_{70} over C_{60}.

Film Structures. The effect of the difference in fullerene molecular structures on the molecular ordering in the composite films was assessed with XRD analyses (Figure S9 in the Supporting Information). The composite films of P3HT:*cis*-2-[70]BIEC, P3HT:bis-[70]BIEC, and P3HT:α-mono-[70]BIEC display sharp diffraction peaks at 2θ = 5.2°, corresponding to the interlayer spacing of P3HT in the out-of-plane profiles, and 2θ = 23.4°, corresponding to the interplanar spacing of P3HT in the in-plane profiles. In-plane XRD patterns of the composite films show broad signals at 2θ = 17−18°, arising from the alignments of the fullerene moieties. All these results indicate the formations of the fullerene alignments and P3HT lamellar structures oriented edge-on with the substrate in the composite films. The more intense signals in the XRD patterns of P3HT:*cis*-2-[70]BIEC and P3HT:α-mono-[70]BIEC than those of P3HT:bis-[70]BIEC may indicate that the regioisomer purity of the fullerene C_{70} compounds affects the alignments of P3HT as well as those of the fullerenes themselves in the composite films.

Meanwhile, the surface morphologies of the composite films were evaluated by AFM (Figure 8). The surface roughnesses increase in the order of P3HT:*cis*-2-[70]BIEC (rms = 3.4 nm) < P3HT:α-mono-[70]BIEC (6.4 nm) < P3HT:bis-[70]BIEC (8.1 nm), suggesting that the fullerene isomer affects the domain size in the composite films. This result is consistent with the degree of the fluorescence quenching of the composite films. Namely, the quenching efficiency of P3HT fluorescence is higher in P3HT:*cis*-2-[70]BIEC (95%) than P3HT:α-mono-[70]BIEC (89%) and P3HT:bis-[70]BIEC (86%) (Figure S10 in the Supporting Information), that is, the excitons generated in the P3HT domains reach to the P3HT−fullerene interface more efficiently in the P3HT:*cis*-2-[70]BIEC with the relatively small domain size. The quenching efficiency of the P3HT fluorescence in P3HT:*cis*-2-[70]BIEC is larger than that in P3HT:*cis*-2-[60]BIEC (90%), although the domain size in the former is larger than that in the latter (rms = 2.1 nm).[19] This may stem from the relatively amorphous nature of *cis*-2-[70]BIEC revealed by the DSC measurement, forming intimately mixed P3HT:fullerene phases with large sizes compared to *cis*-2-[60]BIEC in the composite films.[44]

CONCLUSIONS

In summary, the isomerically pure [70]fullerene *cis*-2 bis-adduct, *cis*-2-[70]BIEC, has been obtained for the first time through the rational tether-directed functionalization and the special separation method by HPLC suitable for fullerene derivatives. A systematic study on the optical, electrochemical, and photovoltaic properties of *cis*-2-[70]BIEC as well as the regioisomer mixture (bis-[70]BIEC) and the corresponding monoadduct (α-mono-[70]BIEC) has been performed to disclose the effects of the pure *cis*-2 regioisomer of C_{70}. Their properties were also compared with those of the BIE−C_{60} adducts to assess the effects of fullerene cage structures. In the BHJ PSC devices with P3HT, *cis*-2-[70]BIEC showed the higher V_{OC} and the PCE than α-mono-[70]BIEC. Compared to the BIE−C_{60} analogue, *cis*-2-[60]BIEC (PCE = 2.8%), the *cis*-2-[70]BIEC-based device has drastic increases in the J_{SC} and PCE (4.2%), which result from the superior light-harvesting and charge separation efficiencies. These results obtained here demonstrate that *cis*-2 isomers of C_{70} bis-adducts are highly promising as excellent electron-acceptors in BHJ PSC devices. The performance of the device based on *cis*-2-[70]BIEC is still inferior to the device with the regioisomer mixture of C_{70}−indene bis-adduct, [70]ICBA (4.8%). Thus, there is still room for the improvement in term of their electron-transporting properties. It can be envisioned that our methodology will open the way for further development on the rational design and isolation of pure regioisomers of fullerene C_{70} bis-adducts as acceptors, which may bring about a remarkable breakthrough in PSC devices.

ASSOCIATED CONTENT

Supporting Information

HPLC profiles, NMR spectra, theoretical chemical shifts, X-ray crystal packing structures, electron densities, TGA, comparison of *cis*-2-[70]BIEC and *cis*-2-[60]BIEC, XRD, and photoluminescence spectra. The Supporting Information is available free of charge on the ACS Publications website at DOI: 10.1021/acsami.5b04351.

AUTHOR INFORMATION

Corresponding Author

*E-mail: imahori@scl.kyoto-u.ac.jp. Fax: +81-75-383-2571. Phone: +81-75-383-2566.

Notes

The authors declare no competing financial interest.

ACKNOWLEDGMENTS

This work is supported by New Energy and Industrial Technology Development Organization (NEDO) and Grand-in-Aid (No. 25220801 to H.I.). The authors thank Micro/NanoFabrication Hub (Kyoto University) for XRD measurements.

REFERENCES

(1) He, Y.; Li, Y. Fullerene Derivative Acceptors for High Performance Polymer Solar Cells. *Phys. Chem. Chem. Phys.* **2011**, *13*, 1970−1983.

(2) Chochos, C. L.; Tagmatarchis, N.; Gregoriou, V. G. Rational Design on n-Type Organic Materials for High Performance Organic photovoltaics. *RSC Adv.* **2013**, *3*, 7160−7181.

(3) Li, Y. Fullerene-Bisadduct Acceptors for Polymer Solar Cells. *Chem. - Asian J.* **2013**, *8*, 2316−2328.

(4) Lai, Y.-Y.; Cheng, Y.-J.; Hsu, C.-S. Applications of Functional Fullerene Materials in Polymer Solar Cells. *Energy Environ. Sci.* **2014**, *7*, 1866−1883.

(5) Umeyama, T.; Imahori, H. Design and Control of Organic Semiconductors and Their Nanostructures for Polymer−Fullerene-Based Photovoltaic Devices. *J. Mater. Chem. A* **2014**, *2*, 11545−11560.

(6) Mazzio, K. A.; Luscombe, C. K. The Future of Organic Photovoltaics. *Chem. Soc. Rev.* **2015**, *44*, 78−90.

(7) Yu, G.; Gao, J.; Hummelen, J. C.; Wudl, F.; Heeger, A. J. Polymer Photovoltaic Cells - Enhanced Efficiencies via a Network of Internal Donor-Acceptor Heterojunctions. *Science* **1995**, *270*, 1789−1791.

(8) Lenes, M.; Wetzelaer, G.-J. A. H; Kooistra, F. B.; Veenstra, S. C.; Hummelen, J. C.; Blom, P. W. Fullerene Bisadducts for Enhanced Open-Circuit Voltages and Efficiencies in Polymer Solar Cells. *Adv. Mater.* **2008**, *20*, 2116−2119.

(9) Lenes, M.; Shelton, S. W.; Sieval, A. B.; Kronholm, D. F.; Hummelen, J. C.; Blom, P. W. M. Electron Trapping in Higher Adduct Fullerene-Based Solar Cells. *Adv. Funct. Mater.* **2009**, *19*, 3002−3007.

(10) Liu, C.; Xiao, S.; Shu, X.; Li, Y.; Xu, L.; Liu, T.; Yu, Y.; Zhang, L.; Liu, H.; Li, Y. Synthesis and Photovoltaic Properties of Novel Monoadducts and Bisadducts Based on Amide Methanofullerene. *ACS Appl. Mater. Interfaces* **2012**, *4*, 1065−1071.

DOI: 10.1021/acsami.5b04351
ACS Appl. Mater. Interfaces 2015, 7, 16676−16685

(11) Wienk, M. M.; Kroon, J. M.; Verhees, W. J. H.; Knol, J.; Hummelen, J. C.; van Hal, P. A.; Janssen, R. A. J. Efficient Methano[70]fullerene/MDMO-PPV Bulk Heterojunction Photovoltaic Cells. *Angew. Chem., Int. Ed.* **2003**, *42*, 3371−3375.
(12) He, Y.; Chen, H.-Y.; Hou, J.; Li, Y. Indene−C_{60} Bisadduct: A New Acceptor for High-Performance Polymer Solar Cells. *J. Am. Chem. Soc.* **2010**, *132*, 1377−1382.
(13) He, Y.; Zhao, G.; Peng, B.; Li, Y. High-Yield Synthesis and Electrochemical and Photovoltaic Properties of Indene-C_{70} Bisadduct. *Adv. Funct. Mater.* **2010**, *20*, 3383−3389.
(14) Liao, S.-H.; Li, Y.-L.; Jen, T.-H.; Cheng, Y.-S.; Chen, S.-A. Multiple Functionalities of Polyfluorene Grafted with Metal Ion-Intercalated Crown Ether as an Electron Transport Layer for Bulk-Heterojunction Polymer Solar Cells: Optical Interference, Hole Blocking, Interfacial Dipole, and Electron Conduction. *J. Am. Chem. Soc.* **2012**, *134*, 14271−14274.
(15) Guo, X.; Cui, C. H.; Zhang, M. J.; Huo, L. J.; Huang, Y.; Hou, J. H.; Li, Y. High Efficiency Polymer Solar Cells Based on Poly(3-hexylthiophene)/Indene-C_{70} Bisadduct with Solvent Additive. *Energy Environ. Sci.* **2012**, *5*, 7943−7949.
(16) Dang, M. T.; Hirsch, L.; Wantz, G.; Wuest, J. D. Controlling the Morphology and Performance of Bulk Heterojunctions in Solar Cells. Lessons Learned from the Benchmark Poly(3-hexylthiophene):[6,6]-Phenyl-C_{61}-butyric Acid Methyl Ester System. *Chem. Rev.* **2013**, *113*, 3734−3765.
(17) Kitaura, S.; Kurotobi, K.; Sato, M.; Takano, Y.; Umeyama, T.; Imahori, H. Effects of Dihydronaphthyl-Based [60]Fullerene Bisadduct Regioisomers on Polymer Solar Cell Performance. *Chem. Commun.* **2012**, *48*, 8550−8552.
(18) Tao, R.; Umeyama, T.; Kurotobi, K.; Imahori, H. Effects of Alkyl Chain Length and Substituent Pattern of Fullerene Bis-Adducts on Film Structures and Photovoltaic Properties of Bulk Heterojunction Solar Cells. *ACS Appl. Mater. Interfaces* **2014**, *6*, 17313−17322.
(19) Tao, R.; Umeyama, T.; Higashino, T.; Koganezawa, T.; Imahori, H. A Single *cis*-2 Regioisomer of Ethylene-Tethered Indene Dimer-Fullerene Adduct as an Electron-Acceptor in Polymer Solar Cells. *Chem. Commun.* **2015**, *51*, 8233−8236.
(20) Sabirov, D. S. Anisotropy of Polarizability of Fullerene Higher Adducts for Assessing the Efficiency of Their Use in Organic Solar Cells. *J. Phys. Chem. C* **2013**, *117*, 9148−9153.
(21) Meng, X.; Zhao, G.; Xu, Q.; Tan, Z. a.; Zhang, Z.; Jiang, L.; Shu, C.; Wang, C.; Li, Y. Effects of Fullerene Bisadduct Regioisomers on Photovoltaic Performance. *Adv. Funct. Mater.* **2014**, *24*, 158−163.
(22) Matsuo, Y.; Kawai, J.; Inada, H.; Nakagawa, T.; Ota, H.; Otsubo, S.; Nakamura, E. Addition of Dihydromethano Group to Fullerenes to Improve the Performance of Bulk Heterojunction Organic Solar Cells. *Adv. Mater.* **2013**, *25*, 6266−6269.
(23) Liao, M.-H.; Lai, Y.-Y.; Lai, Y.-Y.; Chen, Y.-T.; Tsai, C.-E.; Liang, W.-W.; Cheng, Y.-J. Reducing Regioisomers of Fullerene-Bisadducts by Tether-Directed Remote Functionalization: Investigation of Electronically and Sterically Isomeric Effects on Bulk-Heterojunction Solar Cells. *ACS Appl. Mater. Interfaces* **2014**, *6*, 996−1004.
(24) Zhang, B.; Subbiah, J.; Lai, Y.-Y.; White, J. M.; Jones, D. J.; Wong, W. W. H. One-Pot Selective Synthesis of a Fullerene Bisadduct for Organic Solar Cell Applications. *Chem. Commun.* **2015**, *51*, 9837−9840.
(25) Isaacs, L.; Haldimann, R. F.; Diederich, F. Tether-Directed Remote Functionalization of Buckminsterfullerene: Regiospecific Hexaadduct Formation. *Angew. Chem., Int. Ed. Engl.* **1994**, *33*, 2339−2342.
(26) Sander, M.; Jarrosson, T.; Chuang, S.-C.; Khan, S. I.; Rubin, Y. Approaches to Open Fullerenes: Synthesis and Thermal Stability of *cis*-1 Bis(isobenzofuran) Diels-Alder Adducts of C_{60}. *J. Org. Chem.* **2007**, *72*, 2724−2731.
(27) Izquierdo, M.; Ceron, M. R.; Alegret, N.; Metta-Magaña, A. J.; Rodríguez-Fortea, A.; Poblet, J. M.; Echegoyen, L. Unexpected Isomerism in *cis*-2 Bis(pyrrolidino)[60]Fullerene Diastereomers. *Angew. Chem., Int. Ed.* **2013**, *52*, 12928−12931.
(28) Neti, V. S. P. K.; Ceron, M. R.; Duarte-Ruiz, A.; Olmstead, M. M.; Balch, A. L.; Echegoyen, L. High-Yield, Regiospecific Bis-Functionalization of C_{70} Using a Diels-Alder Reaction in Molten Anthracene. *Chem. Commun.* **2014**, *50*, 10584−10587.
(29) Xiao, Z.; Matsuo, Y.; Soga, I.; Nakamura, E. Structurally Defined High-LUMO-Level 66π-[70]Fullerene Derivatives: Synthesis and Application in Organic Photovoltaic Cells. *Chem. Mater.* **2012**, *24*, 2572−2582.
(30) Wong, W. W. H.; Subbiah, J.; White, J. M.; Seyler, H.; Zhang, B.; Jones, D. J.; Holmes, A. B. Single Isomer of Indene-C_{70} Bisadduct-Isolation and Performance in Bulk Heterojunction Solar Cells. *Chem. Mater.* **2014**, *26*, 1686−1689.
(31) Cerón, M. R.; Izquierdo, M.; Aghabali, A.; Valdez, J. A.; Ghiassi, K. B.; Olmstead, M. M.; Balch, A. L.; Wudl, F.; Echegoyen, L. Tethered Bisadducts of C_{60} and C_{70} with Addends on a Common Hexagonal Face and a 12-Membered Hole in the Fullerene Cage. *J. Am. Chem. Soc.* **2015**, *137*, 7502−7508.
(32) Herrmann, A.; Diederich, F.; Thilgen, C.; Termeer, H. U.; Muller, W. H. Chemistry of the Higher Fullerenes - Preparative Isolation of C_{76} By HPLC and Synthesis, Separation, and Characterization of Diels-Alder Monoadducts of C_{70} and C_{76}. *Helv. Chim. Acta* **1994**, *77*, 1689−1706.
(33) van Eis, M. J.; Seiler, P.; Muslinkina, L. A.; Badertscher, M.; Pretsch, E.; Diederich, F.; Alvarado, R. J.; Echegoyen, L.; Pérez Núñez, I. Supramolecular Fullerene Chemistry: A Comprehensive Study of Cyclophane-Type Mono- and Bis-Crown Ether Conjugates of C_{70}. *Helv. Chim. Acta* **2002**, *85*, 2009−2055.
(34) Wong, W. W. H.; Diederich, F. Regio- and Diastereoselective Synthesis of Bis- and Tetrakisadducts of C_{70} by Directed Remote Functionalization Using Tröger Base Tethers. *Chem. - Eur. J.* **2006**, *12*, 3463−3471.
(35) Grossman, R. B.; Doyle, R. A.; Buchwald, S. L. Syntheses of [Ethylene-1,2-bis(η^5-4,5,6,7-tetrahydro-1-indenyl)]zirconium and -Hafnium Hydride Complexes. Improved Syntheses of the Corresponding Dichlorides. *Organometallics* **1991**, *10*, 1501−1505.
(36) Frisch, M. J.; Trucks, G. W.; Schlegel, H. B.; Scuseria, G. E.; Robb, M. A.; Cheeseman, J. R.; Scalmani, G.; Barone, V.; Mennucci, B.; Petersson, G. A.; Nakatsuji, H.; Caricato, M.; Li, X.; Hratchian, H. P.; Izmaylov, A. F.; Bloino, J.; Zheng, G.; Sonnenberg, J. L.; Hada, M.; Ehara, M.; Toyota, K.; Fukuda, R.; Hasegawa, J.; Ishida, M.; Nakajima, T.; Honda, Y.; Kitao, O.; Nakai, H.; Vreven, T.; Montgomery, J. A., Jr.; Peralta, J. E.; Ogliaro, F.; Bearpark, M.; Heyd, J. J.; Brothers, E.; Kudin, K. N.; Staroverov, V. N.; Kobayashi, R.; Normand, J.; Raghavachari, K.; Rendell, A.; Burant, J. C.; Iyengar, S. S.; Tomasi, J.; Cossi, M.; Rega, N.; Millam, J. M.; Klene, M.; Knox, J. E.; Cross, J. B.; Bakken, V.; Adamo, C.; Jaramillo, J.; Gomperts, R.; Stratmann, R. E.; Yazyev, O.; Austin, A. J.; Cammi, R.; Pomelli, C.; Ochterski, J. W.; Martin, R. L.; Morokuma, K.; Zakrzewski, V. G.; Voth, G. A.; Salvador, P.; Dannenberg, J. J.; Dapprich, S.; Daniels, A. D.; Farkas, O.; Foresman, J. B.; Ortiz, J. V.; Cioslowski, J.; Fox, D. J. *Gaussian 09*; Gaussian, Inc.: Wallingford, CT, 2009.
(37) Dang, J.-S.; Wang, W.-W.; Zhao, X.; Nagase, S. Regioselective Derivatization of C_{84} by Diels-Alder Reactions: Applications to Photovoltaic Solar Cells and Fullerene Polymerization. *Org. Lett.* **2014**, *16*, 170−173.
(38) Ni, L.; Yang, W.-W.; Li, Z.-J.; Wu, D.; Gao, X. Regioselective Oxazolination of C_{70}^{2-} and Formation of *cis*-1 C_{70} Adduct with Respect to the Apical Pentagon. *J. Org. Chem.* **2012**, *77*, 7299−7306.
(39) Sun, Q.; Wang, H.; Yang, C.; Li, Y. Synthesis and Electroluminescence of Novel Copolymers Containing Crown Ether Spacers. *J. Mater. Chem.* **2003**, *13*, 800−806.
(40) Zhang, Y.; Yip, H. L.; Acton, O.; Hau, S. K.; Huang, F.; Jen, A. K. Y. A Simple and Effective Way of Achieving Highly Efficient and Thermally Stable Bulk-Heterojunction Polymer Solar Cells Using Amorphous Fullerene Derivatives as Electron Acceptor. *Chem. Mater.* **2009**, *21*, 2598−2600.
(41) Meng, X. Y.; Zhang, W. Q.; Tan, Z. A.; Li, Y. F.; Ma, Y. H.; Wang, T. S.; Jiang, L.; Shu, C. Y.; Wang, C. R. Highly Efficient and Thermally Stable Polymer Solar Cells with Dihydronaphthyl-Based

DOI: 10.1021/acsami.5b04351
ACS Appl. Mater. Interfaces 2015, 7, 16676−16685

[70]Fullerene Bisadduct Derivative as the Acceptor. *Adv. Funct. Mater.* **2012**, *22*, 2187−2193.
(42) Cheng, Y.-J.; Liao, M.-H.; Chang, C.-Y.; Kao, W.-S.; Wu, C.-E.; Hsu, C.-S. Di(4-methylphenyl)methano-C_{60} Bis-Adduct for Efficient and Stable Organic Photovoltaics with Enhanced Open-Circuit Voltage. *Chem. Mater.* **2011**, *23*, 4056−4062.
(43) Han, G. D.; Collins, W. R.; Andrew, T. L.; Bulović, V.; Swager, T. M. Cyclobutadiene−C_{60} Adducts: n-Type Materials for Organic Photovoltaic Cells with High V_{OC}. *Adv. Funct. Mater.* **2013**, *23*, 3061−3069.
(44) Shoaee, S.; Subramaniyan, S.; Xin, H.; Keiderling, C.; Tuladhar, P. S.; Jamieson, F.; Jenekhe, S. A.; Durrant, J. R. Charge Photogeneration for a Series of Thiazolo-Thiazole Donor Polymers Blended with the Fullerene Electron Acceptors PCBM and ICBA. *Adv. Funct. Mater.* **2013**, *23*, 3286−3298.

DOI: 10.1021/acsami.5b04351
ACS Appl. Mater. Interfaces 2015, 7, 16676−16685